INTERNATIONAL JOURNAL OF ENERGY STUDIES

e-ISSN: 2717-7513 (ONLINE); homepage: https://dergipark.org.tr/en/pub/ijes

Research Article

Int J Energy Studies 2025; 10(2): 437-459

DOI: 10.58559/ijes.1616563

Received : 09 Jan 2025
Revised : 07 Mar 2025
Accepted : 24 Mar 2025

Performance analysis and characterization of latent heat storage in ıntegrated thermal management systems under transition season conditions

Gülenay Alevay Kılıç[a*]

[a]*Electrical and Energy Department, Yalova Vocational School, Yalova University, Türkiye, ORCID: 0000-0002-3513-8785*
**gulenay.kilic@yalova.edu.tr*

Highlights

- PCM integration maintained HTF temperatures between 31-34°C under 42% increased heat flux, while achieving a 25% thermal load reduction.
- Thermal stability was demonstrated with only 1.4°C temperature variation between PCM cells.
- The integrated thermal management system maintained the system temperature within the optimum operating range (25-35°C) under varying heat flux loads.
- The PCM's latent heat storage prevented the system from overheating, keeping temperatures below critical limits.

<u>You can cite this article as:</u> Kılıç GA. Performance analysis and characterization of latent heat storage in ıntegrated thermal management systems under transition season conditions. Int J Energy Studies 2025; 10(2): 437-459.

ABSTRACT

Thermal management systems play a crucial role in not only reducing energy losses but also optimizing thermal performance, extending system lifespan, and enhancing energy efficiency. Integrated thermal management systems (TMS) differ from conventional cooling systems by combining active and passive cooling components into a single, unified system, offering a more efficient and sustainable thermal management solution. These systems aim to maximize performance and reliability by ensuring the operation of electronic components, power units, and various industrial equipment within their optimal temperature ranges. In the design of integrated TMS, the influence of different geographical regions and varying climatic conditions emerges as a significant factor. Thus, in addition to current system configurations, the development of customized integrated TMS designs that account for regional climate variations can contribute to improved system performance. In this study, the thermal responses of the radiator, a primary cooling system component of integrated TMS, to transitional seasonal climate conditions were experimentally investigated for two different scenarios. The applied heat fluxes in the scenarios were q"= 9.06 W/cm² and q"= 18.12 W/cm². The thermal behavior of the heat transfer fluid (HTF) and the phase change material (PCM) with latent heat storage capacity was evaluated within the system. The findings revealed that even under a challenging scenario with a 42% increase in HTF inlet temperature, the PCM maintained the system within its optimal temperature range. Moreover, a 25% reduction in thermal load was observed in the system. These results demonstrate that the use of materials like PCM in integrated TMS designs significantly contributes to thermal balance and energy efficiency.

Keywords: Integrated thermal management system, Liquid cooling system, Radiator, Forced heat transfer.

1. INTRODUCTION

The European Commission's "Energy Roadmap 2050" project aims to develop sustainable long-term energy systems for the EU. This roadmap includes objectives such as reducing carbon emissions, enhancing energy efficiency, and promoting the transition to renewable energy sources by 2050. Therefore, the development of energy storage and thermal management technologies is of paramount importance. As a result, Electric Vehicles (EVs) are equipped with various thermal management applications. These systems include direct contact between the battery and coolant or the use of tubes or pipes embedded within the battery through which the coolant flows, indirectly cooling the system. The thermal management systems include air cooling [1], liquid cooling [2], refrigerant cooling [3], Phase Change Material (PCM) cooling [4-5], thermoelectric cooling [6], and heat pipes [7]. Typically, thermal management systems are suited for either cold or hot climates. Hence, assuming similar temperatures across regions can lead to challenges in the operation of thermal management systems (TMS). Moreover, countries and regions with varying climate conditions have distinct thermal management needs for electric vehicles. Consequently, in recent years, there has been a growing trend towards liquid-cooled integrated TMS with dual loops in larger mechanical systems such as electric buses, trains, etc. These applications are evaluated based on performance, weight, size, reliability, protection, energy consumption, and operating conditions. Kharabati and Saedodin (2024) used visualization software in their literature review to identify research trends and gaps for different battery TMS clusters. The findings suggest that integrated cooling systems have become the newest focal point among keywords (frequency of terms in past years). They also note that active and passive cooling systems are present among other cooling methods. Furthermore, in recent years, the keyword "Phase Change Material" has been found to have a high frequency. PCM ensures the system is managed in a stable and balanced manner by storing or releasing heat during phase transitions due to its latent heat storage capacity. Considering that PCMs fall under passive cooling systems, the researchers concluded that there is a focused effort on the design and implementation of "integrated thermal cooling systems" and that PCMs should be used in TMS due to their exceptional performance [8]. Active or passive cooling systems are generally preferred in electric vehicles [9]. Integrated TMS represents a cutting-edge approach that merges the benefits of active and passive cooling strategies. These systems are specifically engineered to manage and dissipate heat produced by high-temperature device components efficiently. Typically, an integrated TMS operates through two distinct cycles. In the primary cycle, heat from the device components is carried to a radiator via a liquid cooling system, where the coolant is subsequently cooled by a dedicated unit.

In the secondary cycle, the fluid circulates through the system, extracting heat from the heat-generating components. This absorbed heat is then transferred to the liquid cooling unit within the primary cycle, ensuring the completion of the thermal regulation process. The secondary cycle interacts with the primary cycle to distribute heat more effectively from the device components and to control the temperature of the device. In an integrated TMS, the radiator is incorporated into the primary cycle's liquid cooling system to facilitate heat transfer. Heat from the components is transferred to the liquid cooling system via the radiator and then cooled by the cooling unit. In this way, the radiator functions as a cooling plate to remove heat generated by the device’s components in the primary cycle [10-12]. This system allows for the regulation of the car's air conditioning and heating based on environmental conditions, ensuring the cabin is either cooled or heated. When cooling of the battery is necessary, the fluid is pumped through a chiller, which functions as a heat exchanger, into the coolant channels of the battery pack [13].

In cold weather conditions, when battery heating is required, warm air is directed into the battery pack through the use of electric heaters or a condenser to sustain the desired operating temperature. One key benefit of liquid-cooled integrated TMS lies in its capacity to offer a broad operating temperature range, enabled by its high thermal conductivity and heat capacity, even under low flow rates. Furthermore, studies have shown that liquid-cooled integrated TMS operates with considerably lower noise levels compared to air-cooled systems [14-17].

An integrated TMS incorporates three types of heat exchangers: a condenser, an evaporator, and a cooler. The condenser is situated ahead of the radiator, while the evaporator is located near the cabin to manage cabin air temperature. The cooler is positioned between the coolant circuit and the battery cooling circuit to streamline the heat exchange process. In their study, Singirikonda and Obulesu (2022) proposed a new design for a two-loop liquid-cooled integrated TMS suitable for both cold and hot climate conditions, as shown in Figure 1. The dual-loop cooling system consists of two water circulation loops: one for primary cooling and the other for machine coolant. Within the liquid coolant loop, the radiator and chiller serve as primary heat exchangers. When the radiator alone cannot effectively handle high ambient temperatures, the chiller is engaged to provide additional cooling. The battery cooling loop and the powertrain cooling loop operate separately in parallel mode, each with its own cooling pumps and tanks.

In this loop, the radiator cools the powertrain components, while the chiller is used to cool the fluid in the battery loop. Both the radiator and chiller work together to cool the battery and powertrain coolants in hot weather conditions. The chiller absorbs heat from the coolant, and the radiator facilitates heat transfer from the coolant to the air. The radiator is a rectangular tube and fin heat exchanger that transfers heat from the coolant to the air. A three-way bypass valve is used to direct the coolant either to the radiator or allow its passage to the chiller. In hot conditions, the heat generated by the powertrain components is used for heat transfer from the coolant to the air through the radiator. The powertrain and cabin coolants are controlled based on weather conditions using coolant pumps and heaters, reducing power consumption. Experimental results from the study showed that the powertrain and cabin temperatures achieved sufficient cooling at external temperatures of −10°C, 30°C, and 40°C. Additionally, the proposed integrated TMS was found to be safe and efficient for both the battery and the vehicle cabin. Unlike traditional liquid cooling or full cooling TMS, which are typically suitable for only one weather condition, the integrated TMS proposed in this study is adaptable to all weather conditions [18].

Recent research has introduced a novel cooling approach incorporating a triple-stage strategy with heat recovery capabilities for electrical systems within an integrated TMS framework. The investigation focused on expanding the operational temperature range while optimizing energy efficiency. Experimental analysis combined with heat pump system testing led to the development of a refined TMS utilizing refrigerant injection technology. Performance validation through AMESim simulations revealed that intermediate heat exchanger-based cooling delivered superior stability compared to dual evaporator configurations. The system demonstrated significant energy savings, ranging from 11.98% to 56.69%, when operating at 35°C ambient temperature with heat recovery implementation. Notably, simulation outcomes indicated a 30% enhancement in energy efficiency under standard cooling conditions, while maintaining effectiveness across diverse temperature zones typical of Chinese climate conditions [19].

A recent study presented an innovative heat pump-based TMS design that effectively maintains thermal equilibrium across diverse environmental conditions. The research utilized comprehensive powertrain modeling to evaluate the system's thermal regulation capabilities. In the operational cycle, high-temperature pressurized refrigerant undergoes condensation in the HVAC circuit's radiator post-compression. The thermal cycle completes as the refrigerant returns to the compressor following heat exchange in the HVAC radiator component. The implementation of frontal air cooling demonstrates superior efficiency in terms of weight reduction and energy conservation compared to conventional liquid cooling methodologies [citation]. Additionally, by utilizing air from the front of the vehicle, models were created for cooling the radiators at high and low temperatures, using ram air (increased air pressure as the vehicle accelerates) and radiator fan models, respectively. High voltage and power electronics module thermal management cycles were designed using circuits with a chiller and radiator to actively control operating temperatures. This model demonstrated that stable thermal management could be achieved under high load driving conditions, particularly during HWFET scenarios (Emission Test Cycles, 2023), even under extreme temperature conditions such as 36°C for high temperatures and 10°C for low temperatures [20].

Waste heat recovery helps improve the positive temperature coefficient by reducing energy consumption during heating. Testing conducted in accordance with NEDC protocols demonstrated that the engine’s thermal recovery mechanism successfully satisfies cabin heating requirements [21]. In this context, He et al. (2023) proposed an integrated thermal management system (TMS) with engine waste heat recovery consisting of two four-way valves in electric vehicles. The experiments and simulations of the integrated TMS model were carried out based on the parameters of each component. Cabin and battery temperatures were examined for 0°C, 20°C, and 40°C. When the proposed integrated TMS cools the battery, the chiller contains low-temperature refrigerant on one side and high-temperature refrigerant on the other side. The system operates more stably and consistently when the ambient temperature falls below 20°C, with different cooling speeds and battery temperatures. Specifically, when the temperature drops below 20°C, part of the high-temperature refrigerant coming from the battery is cooled by the radiator. This cooling is achieved using a cooling water pump in the secondary loop, and since the power consumption is negligible, the overall efficiency of the system is improved. According to the obtained data, the heating and cooling rates of the battery and cabin temperatures in both the heat recovery and non-heat recovery systems were compared. In the heat recovery system, when examining the cooling speeds, it was found that the battery temperature cooled 5.8% faster from 40°C to 30°C, and the cabin temperature cooled 9.7% faster from 40°C to 23°C compared to the non-heat recovery system [22].

Khalili et al. (2023) developed a new integrated thermal management system (TMS) incorporating thermoelectric components and dual radiator configuration was engineered to maintain battery temperatures within the optimal 25-35°C operational range. A model was created to simulate real driving conditions, and results were analyzed using a PID (Proportional-Integral-Derivative) controller and fuzzy logic algorithm. In cold weather, it was observed that the battery surface temperature fluctuated before stabilizing, while in hot weather, the temperature profiles were found to align with the vehicle's speed profile. Through the examination of various system parameters, it was reported that the temperature could be maintained within an appropriate range [23].

High-voltage battery temperature makes it challenging to cool through environmental air in hot climate conditions. Experimental and numerical studies conducted in recent years have shown that radiators commonly used in integrated thermal management systems (TMS) contribute significantly to system efficiency [18-24]. This study presents an experimental investigation aimed at reducing the thermal load on radiators in two-loop liquid-cooled integrated TMS. The study integrates Phase Change Materials (PCMs) into the radiator to reduce the thermal load under moderate seasonal conditions. The thermal behavior characteristics of the radiator and PCM are analyzed, with the obtained data presented in tables and graphs.

2. MATERIAL AND METHOD

2.1. Experimental Procedure

In this study, experiments were conducted in the climate control and cooling laboratory within the university. The proposed thermal management system (TMS) employs dual mechanical cycles for efficient thermal control and heat dissipation from high-temperature device components. The primary circuit utilizes an integrated liquid cooling mechanism for heat removal, while the secondary circuit features a circulating fluid that extracts heat from thermal-generating components before being cooled through the primary loop's liquid cooling unit.The experimental parameters were determined considering the operational conditions of integrated TMSs and climatic factors. The literature indicates that the optimal temperature range for these systems is 25-35°C [20]. Therefore, in the experimental work, the heat fluxes used for two different scenarios were selected as q'' = 9.06 W/cm² and q'' = 18.12 W/cm², respectively, to simulate real operational temperature conditions.

The 42% increase in heat flux in the second scenario was specifically applied to test the system's resistance to high thermal loads. The ambient temperature was set at 22°C (±2), representing the transitional season conditions of the Mediterranean climate zone. This temperature range provides a suitable test environment for evaluating the thermal performance of integrated thermal management systems (TMSs) intended for use in different geographical regions. The externally applied constant wind speed of 6 m/s enhances heat transfer through forced convection, contributing to the cooling performance. Keeping the wind speed constant allowed for a systematic examination of the impact of external environmental conditions on the cooling performance of the system.

In the experimental study, the secondary loop features a radiator integrated with PCM, a fan, and a 2000 W nominal power ceramic thermostatic heater (205 x 45 x 35 mm in size) with PTC insulation. Additionally, two air intake/exhaust dampers are used. PCM, utilized in both cooling and heating applications, exploits its latent heat storage capacity to either store or release thermal energy from the fluid in thermal contact. This ensures that the system's operating temperature remains constant, or when necessary, heat is released back into the system to maintain a stable state.

When selecting the PCM, it is crucial to match its solidification/melting temperature range with the system's operating temperature range. In this study, as the optimal operating temperature range for the batteries in the TMS is between 25–35°C [23], the working temperature range for the alcohol-based PCM fluid used in the system is synthesized to be between 34°C and 44°C. This choice ensures that the PCM remains stable in its solid phase at 34°C, beginning latent heat storage before entering the mushy zone.

In the experiments, the effect of wind on cooling the radiator is enhanced using an external axial fan (Figure 1a). The specifications of the axial fan used are as follows: voltage 220V, frequency 50Hz, speed 1350 rpm, airflow 17,400 m^3/h, and power 210 W. The heat transfer fluid circulating inside the radiator is air. Figure 1(b) displays the top view of the experimental setup, with the following labeled components: A - radial fan, B - heater, C - HTF inlet temperature sensor position, D - radiator, E - HTF outlet temperature sensor position, F - PCM first cell temperature sensor position, G - ambient airflow measurement device (anemometer), and H - PCM final cell temperature sensor position. Figure 1(c) provides the front view of the experimental setup.

During the design phase, to ensure that the necessary and sufficient conditions were met, the primary goal was to maintain uninterrupted flow through the HTF channels. Additionally, in the radiator design, the pool structure where the PCM is placed was designed to maximize the benefit from the latent heat storage capacity of the PCM by increasing the surface area. The radiator dimensions were manufactured based on its exact industrial application, as shown in Figure 2. The diameter of the radiator inlet and outlet neck channels is 50 mm, and the volumes of PCM, circulating HTF, and the aluminum body are 3737.5 cm^3, 4115.8 cm^3, and 1831 cm^3, respectively.

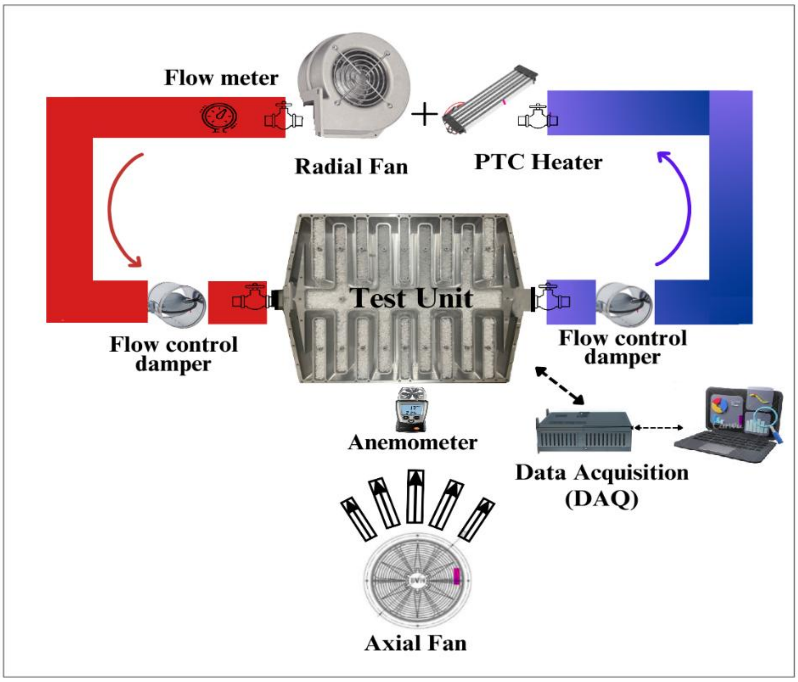

(a)

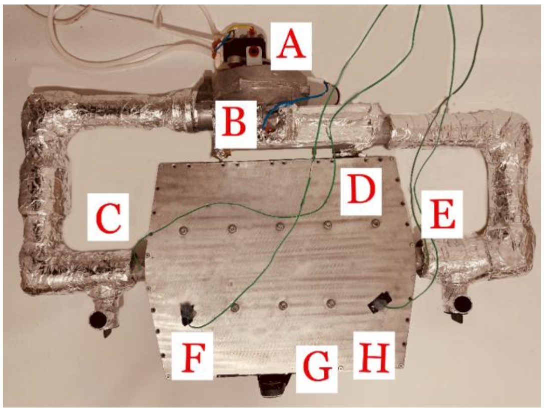

(b)

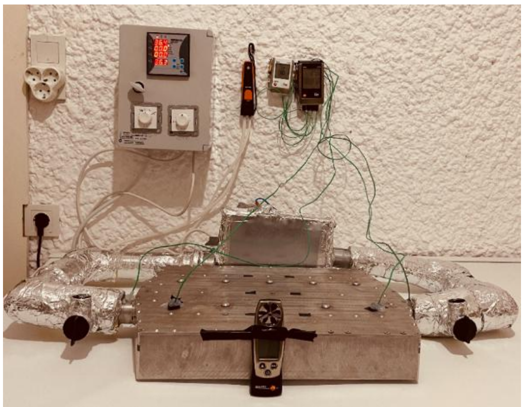

(c)

Figure 1. (a) Schematic of the test section (b) Top view of the setup: A radial fan, B PTC heater, C HTF inlet temperature sensor, D radiator, E HTF outlet temperature sensor, F PCM first cell temperature sensor, G anemometer, H PCM last cell temperature sensor (c) Front view

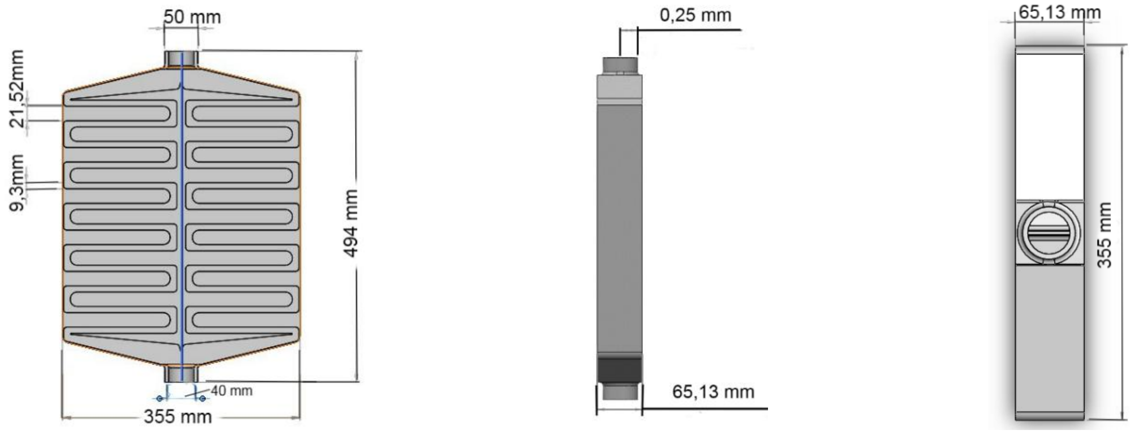

(a) (b) (c)

Figure 2. Test section outer and inner section dimensions (a) top view (b) right view (c) Front view

Table 1. Thermophysical properties of PCM and HTF [25]

Properties, Unit	**PCM**	**HTF**
Solidification/melting temperature °C	34/44	-
$L_{s/m}$, kJ/kg	218.4	-
C_p, kJ/kg K	2.41	0.24
ρ, kg/m^3	824	1.204
k, W/mK	0.2	0.0221
μ, kg/ms	10	1.79x10^{-5}

In the study, an alcohol-based PCM with a wide melting/freezing temperature range was selected. The PCM's thermophysical characteristics are presented in Table 1. Since the PCM and HTF do not directly contact each other, heat transfer occurs along the setup via conduction and convection. The HTF inlet/outlet temperatures, PCM first/last cell temperatures, HTF velocity/volumetric flow rate, HTF static/total pressure values, and ambient temperatures were recorded with a data logger. The wind speed supplied externally to the system is 6 m/s on average, and the variation of wind speed with time is shown in Figure 3. The HTF volumetric flow rate and system total pressure distribution over time are shown in Figure 4.

The ambient temperature was selected based on the assumption of transitional climate conditions dominant in the Mediterranean region and is approximately 22 °C (±2). The time-dependent ambient temperature distributions for the scenarios are shown in Figure 5. During the experiments, HTF was heated using a 2400 W resistance integrated into the radial fan with forced convection, and circulation was maintained at ~40 °C. Prior to subsequent tests, a 6-hour interval was implemented to eliminate residual thermal loads from setup walls. Temperature measurements from the first and last PCM cells along the right axis were recorded every 5 seconds, utilizing the radiator's symmetrical design.The boundary conditions used in the scenarios are detailed in Table 2.

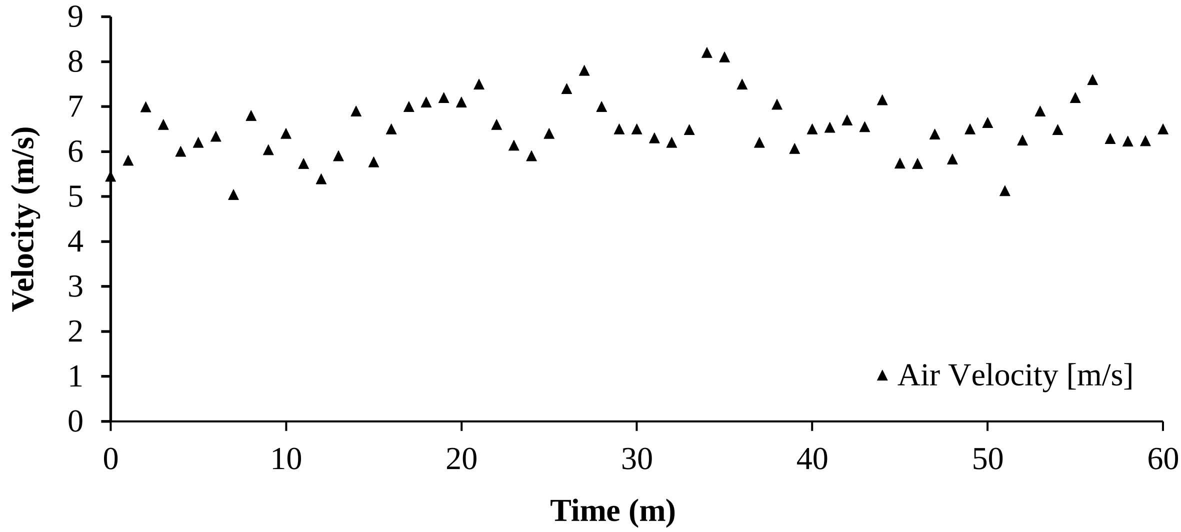

Figure 3. The time-dependent distribution of external wind speed.

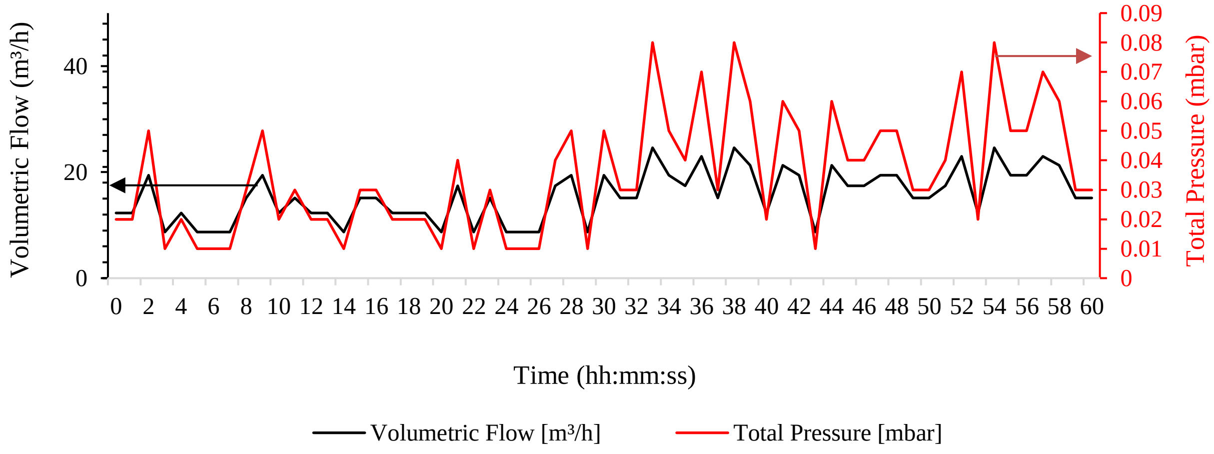

Figure 4. Time-dependent volumetric flow rate and total pressure values

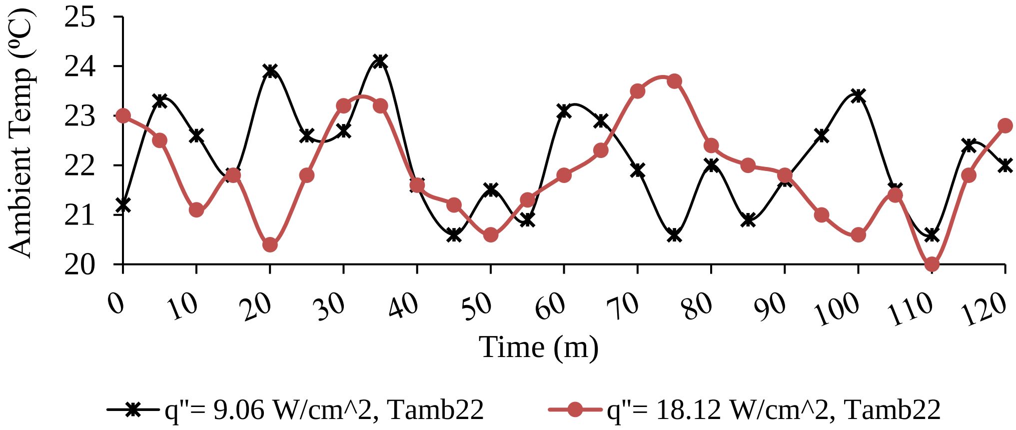

Figure 5. Senaryolardaki zamana bağlı ortam sıcaklık dağılımları

Table 2. Boundary conditions

Senaryo	**1**	**2**
Heat Flux, q''	9.06 W/cm^2	18.12 W/cm^2
Reynolds number	5720	
Ambient temperature	22 (±2)°C	
The avg. volumetric flow rate of HTF	12.8 m^3/h	
Static avg. pressure	0.03 mbar	
HTF velocity	1.7 m/s	

2.2. Uncertainty Analysis

Uncertainty analysis in experimental studies plays a significant role in the reliability of the experiment. One important aspect to consider in experiments is distinguishing between systematic errors and random errors. Experimental uncertainty types are generally divided into two categories. These include errors originating from the experimental setup configuration and measurement equipment limitations, as well as errors introduced by human factors during experimentation. The first type of errors affect the uncertainty of the experimental results and are calculated using Equations 1-4 [26].

$$W_{T_{fg}} = \sqrt{[(a_1)^2 + (b_1)^2 + (c_1)^2 + (e_1)^2]} \tag{1}$$

$$W_{T_c} = \sqrt{[(a_1)^2 + (b_1)^2 + (c_1)^2 + (l_1)^2]} \tag{2}$$

$$W_{T_s} = \sqrt{[(a_2)^2 + (c_2)^2]} \tag{3}$$

$$W_{c_v} = \sqrt{[(v_1)^2 + (x_1)^2]} \quad (4)$$

Systematic errors maintain consistency across all readings during experimentation and can be mitigated through proper calibration and correction procedures. In the uncertainty calculations, W denotes the overall uncertainty value, while W_ρ and W_{cp} represent potential errors in reading tabulated physical property values. The various error components include: internal temperature (T_{fg}), ambient temperature (T_c), time in temperature measurement (T_s), thermocouple pair errors (a_1), digital thermometer errors (b_1), connection components and points errors (c_1), average fan inlet temperature measurement errors (e_1), ambient or experimental environment temperature measurement errors (l_1), time value reading errors (a_2), and periodic temperature reading average errors (c_2). For this particular study, the total uncertainty in temperature measurements falls within a range of 0.1 to ±0.648 °C, which is considered to be within acceptable limits for the research objectives. [26].

2.3. Economic Analysis Method

The Life Cycle Cost (LCC) method is employed to calculate the total costs associated with the initial, operating, and maintenance phases of a system. The primary objective of LCC analysis is to identify the most cost-effective solution from a range of alternatives, aiming to minimize the long-term ownership costs. The LCC approach integrates both the acquisition and operational costs, providing a comprehensive financial evaluation over the system's lifetime. This method emphasizes long-term financial considerations in the economic assessment of systems. To evaluate the Life Cycle Cost (LCC), different financial assessment methods are available, including Net Present Value (NPV) and Internal Rate of Return (IRR). In this research, the NPV methodology is employed to conduct an economic comparison of the systems described below. This method converts all costs and benefits into present value (PV), with the highest NPV alternative being identified as the most economically viable option. The NPV can be mathematically expressed as follows [5, 27, 28]:

$$PV = PV\ (Benefits) - PV\ (Costs) \quad (1)$$

$$NPV = \sum_{n=k+1}^{t} \frac{B_n}{(1+i)^n} - \sum_{n=0}^{k} \frac{C_n}{(1+i)^n} \quad (2)$$

In the equation above, B_n and C_n represent the benefit and cost values respectively over the system's lifespan (n years), while i represents the annual interest rate. Since no cash inflow is involved in this analysis, the benefit term (B_n) in Equation (2) is set to zero. Therefore, only the cost term in Equation (1) is considered. The main cost components include the initial investment for the Thermal Management System (TMS), encompassing both installation and operational electricity costs. The analysis excludes repair and maintenance costs, as well as salvage values, as these are assumed to be equivalent for both systems under comparison. The systems are evaluated over a lifespan (n) of 10 years, with an annual interest rate of 10%. [29-30].

3. RESULTS AND DISCUSSIONS

In this experimental study, Phase Change Material (PCM) was integrated into the air-cooled radiator in the liquid-cooled system used in the primary loop of the integrated thermal management system (TMS). This integration aimed to reduce the thermal load on the radiator. According to the experimental results, the temperature difference between the inlet and outlet of HTF (ΔT_{HTF}) was examined over time for both scenarios, as shown in Figure 6. The data showed that the HTF outlet temperature decreased for both scenarios by 8.77% and 24.89%, respectively. For Scenario 2, ΔT_{HTF} was calculated to be 8.46 °C. As shown in Table 3, in Scenario 2, the cooling load in the radiator with the integrated TMS was reduced by 24.89%. This study demonstrates that the latent heat storage method integrated into radiators used in integrated thermal management systems will positively impact the existing cooling process.

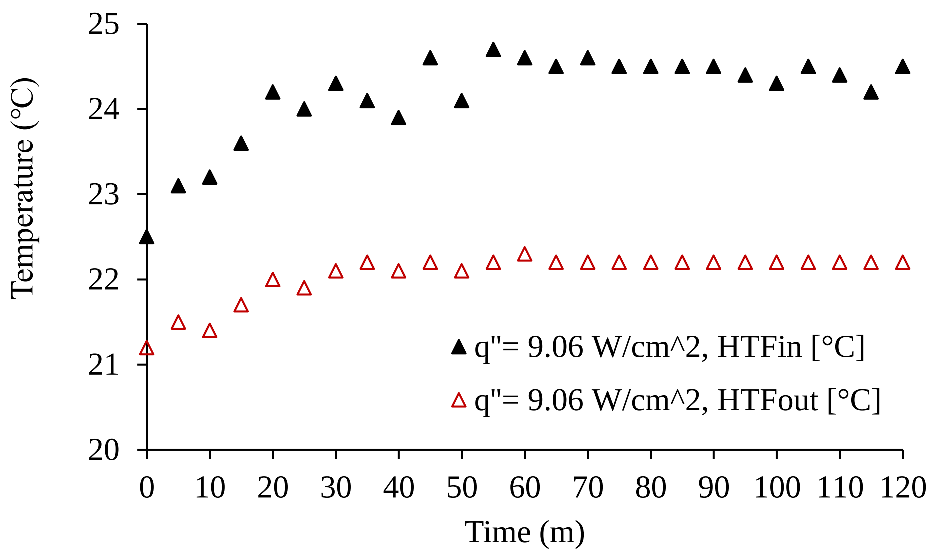

(a)

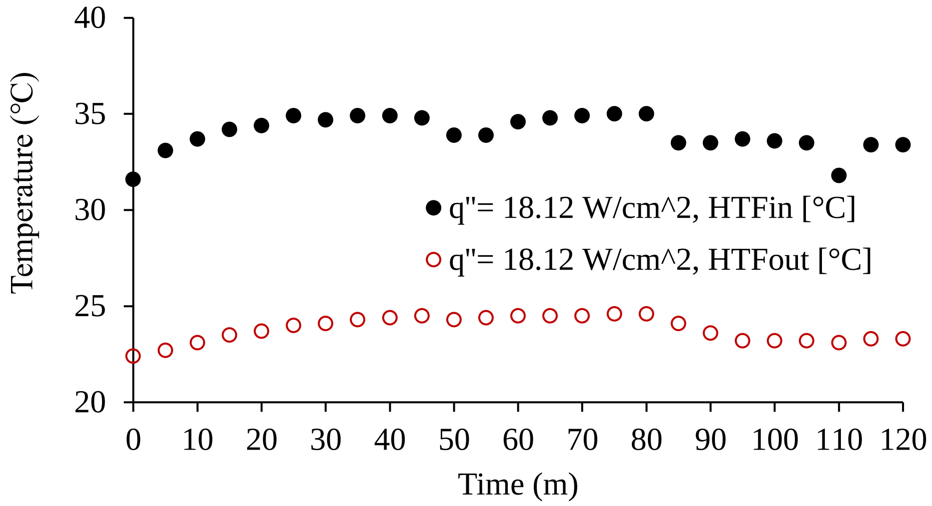

(b)

Figure 6. The distribution of the HTF_{inlet} and HTF_{outlet} temperatures **(a)** q''= 9.06 W/cm^2 **(b)** q''= 18.12 W/cm^2

Table 3. Temperature difference ratios of HTF_{inlet} and HTF_{outlet}

Scenario	q''= 9.06 W/cm^2		q''= 18.12 W/cm^2	
HTF (ºC)	in	out	in	out
Average (ºC)	24.2	22.1	34.0	25.5
Ratio	-8.77%		-24.89%	

According to the data presented in Table 4, PCM temperature in the first cell remained within the range of 22-25°C throughout the experiment. The PCM temperature distribution shown in Figure 7 was examined for two different conditions. In Scenario 1, shown in Figure 7a, the temperature difference between the first and last cells was measured as an average of 0.2°C. In Scenario 2, shown in Figure 7b, this difference reached 2.09°C. The primary reasons for this temperature difference were identified: the effect of the 25.56 cm distance between the chambers on heat transfer via conduction and convection, and the impact of the simulated external wind speed on the system. When considering all the results, the low temperature difference between the cells indicates that a homogeneous thermal distribution is maintained in the system. During the phase change of PCM, its latent heat storage property played an essential role in the thermal performance of the system. As a result, heat energy from the environment was absorbed by the PCM, preventing the system temperature from rising.

Table 4. Temperature difference ratios in the first and last cells of PCM

Scenario	q''= 9.06 W/cm^2		q''= 18.12 W/cm^2	
PCM (ºC)	in	out	in	out
Average (ºC)	22.4	22.0	25.5	23.4
Ratio	-1.96%		-8.19%	

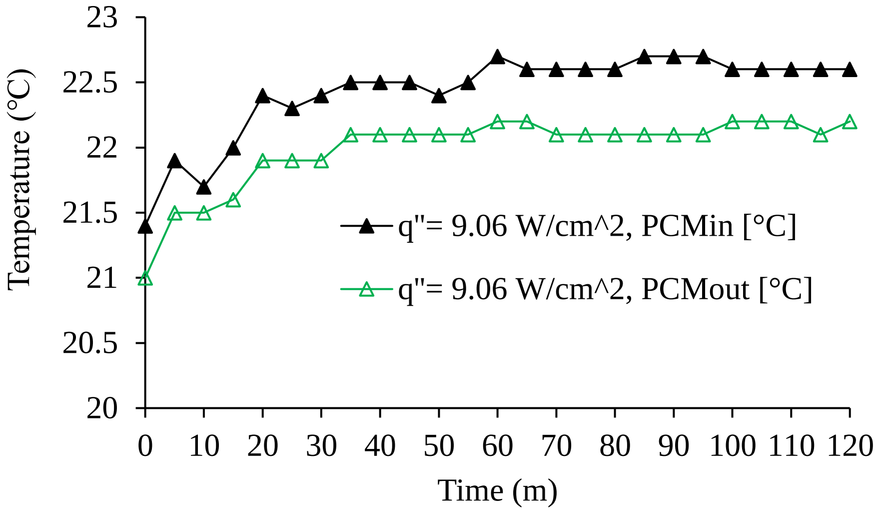

(a)

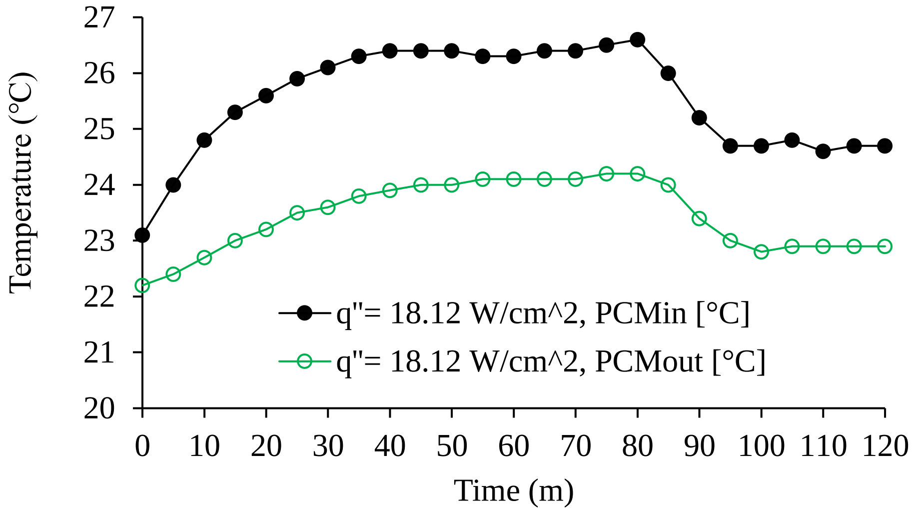

(b)

Figure 7. The temperature spread of the PCM in the first and last cells. **(a)** q''= 9.06 W/cm^2 **(b)** q''= 18.12 W/cm^2

The obtained results align with the current literature and contribute to expanding the knowledge base by presenting new findings and analyses. For instance, He et al. (2023) [23] found that when cabin and battery temperatures rise above 40 °C, a portion of the high-temperature coolant leaving the battery is cooled 5.8% faster (from 40 ℃ to 30 ℃) through the cooling water and radiator in the secondary loop. In light of the data from this study, it contributes to targeting lower temperatures than the upper limit of the optimum range, which is 30 ℃. Furthermore, the rapid temperature absorption by the PCM and the fact that the HTF does not exceed 30 ℃ suggests that the secondary loop cooling water pump could operate less frequently. Additionally, the positive effect of the PCM on thermal stability [5] demonstrates that thermal stability can be maintained even in warm seasons.

In Figure 8, both scenarios are compared, and Figure 8 (a) shows the time-dependent changes in the HTF inlet temperatures. In Scenario 1, with a heat flux of 9.06 W/cm², the HTF inlet temperature enters the system at approximately 24°C and maintains a stable temperature. In contrast, in Scenario 2, with a heat flux of q'' = 18.12 W/cm², the HTF inlet temperature enters the system at around 34°C and stabilizes at a higher temperature range. Figure 8 (b) presents the time-dependent changes in the HTF outlet temperatures. In Scenario 1, the outlet temperatures remain stable between 22-24°C. However, despite the higher inlet temperature in Scenario 2, the outlet temperatures only rise between 23-27°C. The results clearly show the strong performance of the PCM's latent heat storage capacity. Despite a 42% increase in the heat flux in Scenario 2, the HTF outlet temperature only increased by 1-3°C due to the PCM. This indicates that the PCM effectively balanced the high temperature differences and successfully activated its latent heat storage capacity.

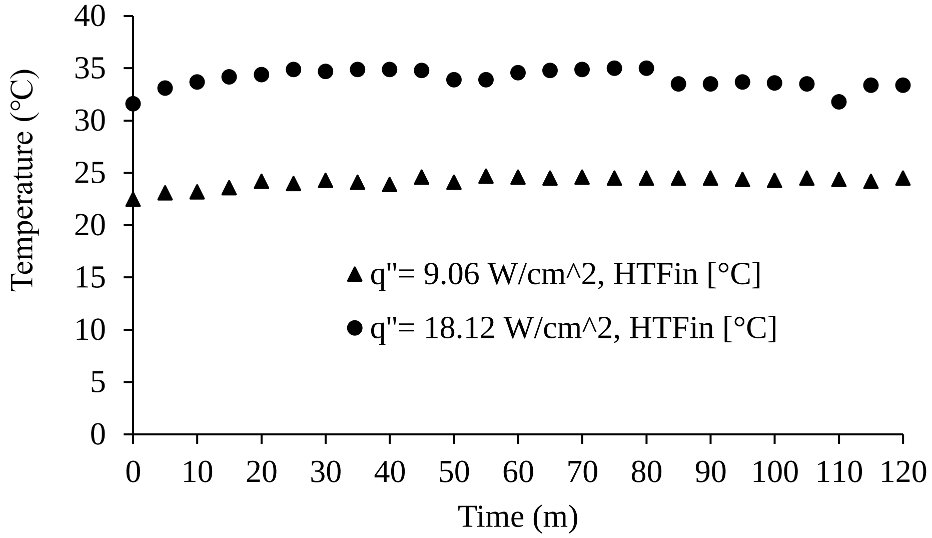

(a)

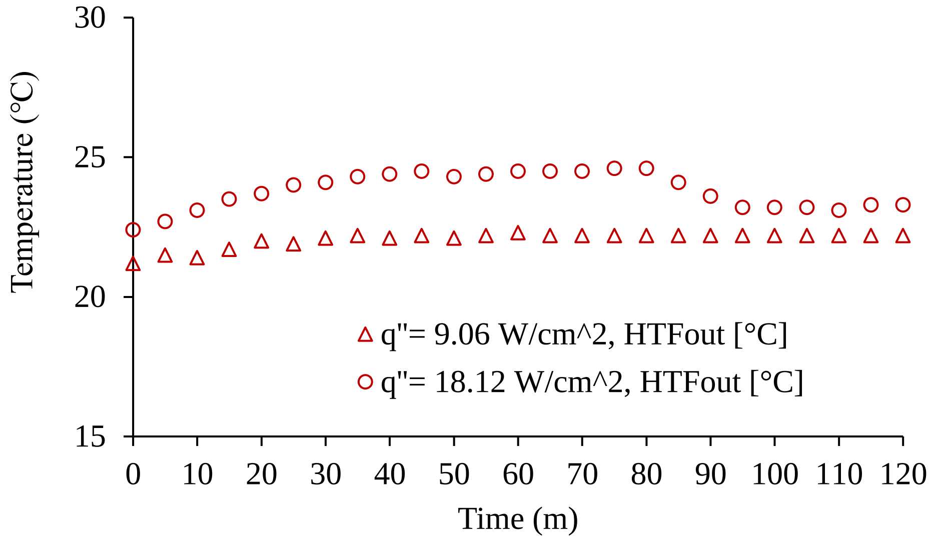

(b)

Figure 8. Comparison of temperature distributions for both scenarios **(a)** HTF_{in} **(b)** HTF_{out}

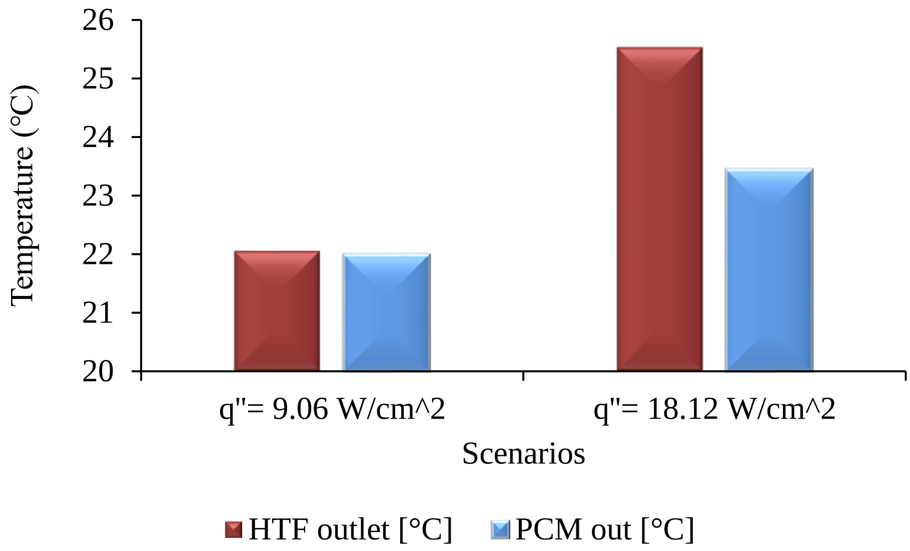

Figure 9. Distribution of average exit temperatures of HTF and PCM in the scenarios.

When Figure 9 is examined, the effects of the 42% increase in HTF inlet temperature on the system are clearly visible. In Scenario 1, both HTF and PCM exit temperatures show an ideal thermal match at 22°C, while in Scenario 2, the HTF exit temperature increased to 25.7°C and the PCM exit temperature was measured at 23.4°C. The increase in HTF exit temperature was limited to 3.7°C (16.8%), while the increase in PCM exit temperature was only 1.4°C (6.4%). These results demonstrate that the thermal buffering effect of PCM is working effectively. In particular, the much lower increase in PCM exit temperature compared to HTF confirms that the selected PCM's latent heat storage capacity is being used efficiently and system stability is maintained. This data clearly shows that proper PCM integration significantly enhances the system's resistance to thermal shocks.

4. CONCLUSION

In this study, an experimental investigation was conducted on the importance and performance of the integrated TMS. The effects of integrating PCM into the radiator, which is part of a liquid-cooled system in the secondary loop frequently used in the literature, on thermal management were examined under two different thermal loads. The study aimed to decrease the thermal load on the radiator under transitional season climate conditions by using the latent heat storage capacity of the PCM. The experimental conditions were selected based on the optimal operating temperature range (25-35°C) for integrated TMS reported in the literature, and two different heat fluxes, namely q''= 9.06 W/cm² and q''= 18.12 W/cm², were used. The results include an examination of the HTF inlet/outlet temperature differences, temperature differences between cells containing PCM integrated into the radiator, uncertainty analysis, economic analysis, and the effectiveness of thermal management within the system.

When evaluating the data obtained in this study:

- The radiator outlet temperature within the integrated TMS decreased by approximately 25%.
- When examining the PCM temperature values and temperature rise rates, latent heat storage energy was utilized in the mushy zone, and the temperature in the last cell of the radiator did not exceed 25°C.
- The risk of damage due to overheating was reduced, and even in a challenging scenario with a 42% increase in heat flux, the HTF outlet temperature was maintained in the range of 31-34°C.
- The temperature difference between the first and last PCM cells remained within 1.4°C. This indicates that the temperature remained stable throughout the radiator channels.
- The calculated uncertainty analysis values demonstrate that the study falls within acceptable limits, thereby increasing the reliability of the obtained results.

These results strongly support the potential of proper PCM selection to enhance energy efficiency in heat management applications. This demonstrates the effectiveness of thermal energy transfer thanks to PCM's latent heat storage capability. Additionally, maintaining a constant external temperature and wind speed has limited the influence of environmental conditions, thus increasing the reliability of the experimental data.

When the economic analysis of this system was conducted, it was observed that although PCM integration increases initial investment costs compared to standard radiators, it results in significant energy savings in cooling system consumption due to a reduction in thermal load by up to 25%. Furthermore, reducing thermal stress on system components prolongs equipment lifespan and reduces maintenance costs. These advantages balance the initial investment cost of the system in the medium term [24].

Future studies will investigate the integration of the radiator with a heat exchanger in the secondary loop and explore thermal and flow dynamics using PCMs with different thermal properties. Additionally, more comprehensive studies conducted under various climate conditions and with different types of PCMs will enable further advancements in integrated thermal management systems.

DECLARATION OF ETHICAL STANDARDS

The authors of the paper submitted declare that nothing which is necessary for achieving the paper requires ethical committee and/or legal-special permissions.

CONTRIBUTION OF THE AUTHORS

Gulenay Alevay Kilic: Conceptualization, methodology, software, validation, formal analysis, investigation, data curation, writing, visualization

CONFLICT OF INTEREST

There is no conflict of interest in this study.

REFERENCES

[1] Lajunen A, Yang Y, Emadi A. Recent developments in thermal management of electrified powertrains. IEEE Transactions on Vehhicular Technology 2018; 67: 11486–11499. https://doi.org/10.1109/TVT.2018.2876315

[2] Tang X, Guo Q, Li M, Wei C, Pan Z, Wang Y. Performance analysis on liquid cooled battery thermal management for electric vehicles based on machine learning. Journal of Power Sources 2021; 494: 229-727. https://doi.org/10.1016/j.jpowsour.2021.229727

[3] Guo J, Jiang F. A novel electric vehicle thermal management system based on cooling and heating of batteries by refrigerant. Energy Conversion Management 2021; 237: 114-145. https://doi.org/10.1016/j.enconman.2021.114145

[4] Yuksel, A. (2025). Performance evaluation of PCM integration in primary healthcare centers under different climate conditions: A multi-criteria decision-making approach. Journal of Energy Storage, 124, 116853. https://doi.org/10.1016/j.est.2025.116853

[5] Kilic GA, Yalcin E, Aydin AA. Optimum Operating Temperature Range of Phase Change Materials Used in Cold Storage Applications: A Case Study. In: Dincer, I., Colpan, C., Ezan, M. (eds) Environmentally-Benign Energy Solutions Green Energy and Technology. Springer, Cham, Switzerland AG, (2020). https://doi.org/10.1007/978-3-030-20637-6_35

[6] Lyu Y, Siddique ARM, Majid SH, Biglarbegian M, Gadsden SA, Mahmud S. Electric vehicle battery thermal management system with thermoelectric cooling. Energy Reports 2019; 5: 822–827. https://doi.org/10.1016/j.egyr.2019.06.016

[7] Bernagozzi M, Georgoulas A, Mich´e N, Rouaud C, Marengo M. Novel battery thermal management system for electric vehicles with a loop heat pipe and graphite sheet inserts. Applied Thermal Engineering 2021; 194: 117061, 1-16. https://doi.org/10.1016/j.applthermaleng.2021.1170

[8] Kharabati S, Saedodin S. A systematic review of thermal management techniques for electric vehicle batteries. Journal of Energy Storage 2024; 75: 109586, 1-58 https://doi.org/10.1016/j.est.2023.109586

[9] Zou H, Jiang B, Wang Q, Tian C, Yan Y. Performance analysis of a heat pump air conditioning system coupling with battery cooling for electric vehicles. Energy Procedia 2014; 61: 891–894. https://doi.org/10.1016/j.egypro.2014.11.989

[10] Behi H, Karimi D, Behi M, Ghanbarpour M, Jaguemont J, Sokkeh MA, Gandoman FH, Berecibar M, Van Mierlo J. A new concept of thermal management system in Li-ion battery using air cooling and heat pipe for electric vehicles. Applied Thermal Engineering 2020; 174: 115280, 1-14. https://doi.org/10.1016/j.applthermaleng.2020.115280

[11] Kuang X, Li K, Xie Y, Wu C, Wang P, Wang X, Fu C. Research on control strategy for a battery thermal management system for electric vehicles based on secondary loop cooling. IEEE Access 2020; 8: 73475–73493. https://doi.org/10.1109/ACCESS.2020.2986814

[12] Leighton D. Combined fluid loop thermal management for electric drive vehicle range improvement. SAE International Journal of Passenger Cars Mechanical System, National Renewable Energy Laboratory (NREL); 8: 5400–63430, Golden, CO USA, 2015. https://doi:10.4271/2015-01-1709

[13] Wang J, Lu S, Wang Y, Ni Y, Zhang S. Novel investigation strategy for minichannel liquid-cooled battery thermal management system. International Journal of Energy Research 2020; 44: 1971–1985. https://doi.org/10.1002/er.5049

[14] Chung Y, Kim MS. Thermal analysis and pack level design of battery thermal management system with liquid cooling for electric vehicles. Energy Conversion and Management 2019; 196: 105–116. https://doi.org/10.1016/j.enconman.2019.05.083

[15] Pesaran AA, Keyser M. Thermal characteristics of selected EV and HEV batteries.16th Annual Battery Conference on Applications and Advances, Long Beach, CA, USA, 2022.

https://ieeexplore.ieee.org/abstract/document/905129. Access date: 09 Dec 2024. https://doi.org/10.1109/BCAA.2001.905129

[16] Siddique ARM, Mahmud S, Heyst BV. A comprehensive review on a passive (phase change materials) and an active (thermoelectric cooler) battery thermal management system and their limitations. Journal of Power Sources 2022; 401: 224-237. https://doi.org/10.1016/j.jpowsour.2018.08.094

[17] Liu C, Li F, Ma LP, Cheng HM. Advanced materials for energy storage. Advanced Materials 2010; 22(8): 28-62. https://doi.org/10.1002/adma.200903328

[18] Singirikonda S, Obulesu YP. Adaptive secondary loop liquid cooling with refrigerant cabin active thermal management system for electric vehicle. Journal of Energy Storage 2022; 50: 104624, 1-17. https://doi.org/10.1016/j.est.2022.104624

[19] Yang H, Wu J, Xue X, Guo Z, Zhang H, Chen F, Chen Y. A refrigerant-injection heat pump-based efficient integrated thermal management system for electric vehicles approaching the wide temperature range in China. Energy Conversion and Management 2023; 288: 117102, 1-21. https://doi.org/10.1016/j.enconman.2023.117102

[20] Bae E, Hyun J, Han DJ. Adaptive Integrated Thermal Management System for a Stable Driving Environment in Battery Electric Vehicles. Batteries 2024; 10(2): 59, 1-26. https://doi.org/10.3390/batteries10020059

[21] Emission Test Cycles, 2023. Available online: https://dieselnet.com/standards/cycles/hwfet.php. Access date: 11 Nov 2024.

[22] He L, Gu Z, Zhang Y, Jing H, Li P. Control strategy analysis of vehicle thermal management system based on motor heat utilization. Energy Technology 2023; 11(10): 2300495. https://doi.org/10.1002/ente.202300495

[23] Khalili H, Ahmadi P, Ashjaee M, Houshfar E. Thermal analysis of a novel cycle for battery pre-warm-up and cool down for real driving cycles during different seasons. Journal of Thermal Analysis and Calorimetry 2023; 148(16): 8175-8193. https://doi.org/10.1007/s10973-022-11601-3

[24] Kilic GA. An experimental analysis on the effects of passive liquid cooling system on thermal management system. International Journal of Thermofluids 2023; 18: 100370. https://doi.org/10.1016/j.ijft.2023.100370

[25] Cong R, Zhang H, Xu C, Fang G. Thermal properties of myristyl alcohol/polyvinyl butyral/carbon nanotubes as composite phase change materials for thermal energy

storage. International Journal of Energy Research 2022; 46(11): 15804-15815. https://doi.org/10.1002/er.8279

[26] Işık S, Yıldız C. Improving thermal energy storage efficiency of solar collector tanks by placing phase change materials in novel finned-type cells. Thermal Science and Engineering Progress 2020; 19: 100618. https://doi.org/10.1016/j.tsep.2020.100618

[27] Jaguemont J, Van Mierlo J. A comprehensive review of thermal management systems for battery electric vehicles. Journal of Energy Storage 2020; 131: 110001. https://doi.org/10.1016/j.est.2020.101551

[28] Luerssen C, Gandhi O, Reindl T, Sekhar C, Cheong D. Life cycle cost analysis (LCCA) of PV-powered cooling systems with thermal energy and battery storage for off-grid applications. Applied Energy 2020; 273: 115145, 1-18. https://doi.org/10.1016/j.apenergy.2020.115145

[29] Altuntas O, Sogut MZ, Yalcin E, Karakoc TH. Assessment of thermodynamic and environmental performances in subcooling process for different refrigerants. International Journal of Exergy 2017; 24(2-4); 216-234. https://doi.org/10.1504/IJEX.2017.087655